THE JOURNAL OF BIOLOGICAL CHEMISTRY
Vol. 278, No. 52, Issue of December 26, pp. 52461–52470, 2003
Printed in U.S.A.

Structure of *Plasmodium falciparum* Triose-phosphate Isomerase-2-Phosphoglycerate Complex at 1.1-Å Resolution*

Received for publication, August 4, 2003, and in revised form, October 10, 2003
Published, JBC Papers in Press, October 16, 2003, DOI 10.1074/jbc.M308525200

Sampathkumar Parthasarathy‡§, Kandiah Eaazhisai‡, Hemalatha Balaram¶, Padmanabhan Balaram‡, and Mathur R. N. Murthy‡‖

From the ‡Molecular Biophysics Unit, Indian Institute of Science, Bangalore 560 012, and ¶Molecular Biology and Genetics Unit, Jawaharlal Nehru Center for Advanced Scientific Research, Jakkur, Bangalore 560 064, India

Triose-phosphate isomerase, a key enzyme of the glycolytic pathway, catalyzes the isomerization of dihydroxy acetone phosphate and glyceraldehyde 3-phosphate. In this communication we report the crystal structure of *Plasmodium falciparum* triose-phosphate isomerase complexed to the inhibitor 2-phosphoglycerate at 1.1-Å resolution. The crystallographic asymmetric unit contains a dimeric molecule. The inhibitor bound to one of the subunits in which the flexible catalytic loop 6 is in the open conformation has been cleaved into two fragments presumably due to radiation damage. The cleavage products have been tentatively identified as 2-oxoglycerate and *meta*-phosphate. The intact 2-phosphoglycerate bound to the active site of the other subunit has been observed in two different orientations. The active site loop in this subunit is in both open and "closed" conformations, although the open form is predominant. Concomitant with the loop closure, Phe-96, Leu-167, and residues 208–211 (YGGS) are also observed in dual conformations in the B-subunit. Detailed comparison of the active-site geometry in the present case to the *Saccharomyces cerevisiae* triose-phosphate isomerase-dihydroxy acetone phosphate and *Leishmania mexicana* triose-phosphate isomerase-phosphoglycolate complexes, which have also been determined at atomic resolution, shows that certain interactions are common to the three structures, although 2-phosphoglycerate is neither a substrate nor a transition state analogue.

Triose-phosphate isomerase (TIM)[1] is a ubiquitous glycolytic enzyme that catalyzes the isomerization of dihydroxy acetone phosphate (DHAP) and glyceraldehyde 3-phosphate through the intermediate formation of *cis*-enediol(ate(s)). Commenting on the catalytic efficiency of TIM, Knowles (1) states "This enzyme (TIM) appears to have arrived at the end of its evolutionary development as a catalyst." It has been argued that the evolutionary pressure for TIM to be a perfect catalyst has been intense, since for "flight or fight" there is an instant requirement for muscle ATP. The catalytic reaction of TIM is chemically simple and involves intermolecular protonation and deprotonation between the enzyme and substrate. The enzyme achieves the proton transfers with the help of certain elements as catalytic tools, a 10-residue loop that closes over the active site and stabilizes the reaction intermediate and a catalytic base and an acid to perform the enolization steps (1). It is believed that catalysis is a result of stronger binding of the enzyme to its transition state than to the initial enzyme-substrate complex (2). Although various schemes for this reaction have been proposed (for a review of the schemes, see Cui and Karplus (3)), the most frequently discussed mechanism is the one that involves Glu-165 as the catalytic base in the first proton transfer and His-95 as the catalytic acid for the rest of the reaction (3) (Fig. 1*a*). Despite numerous experimental (4–9) and theoretical studies (10, 11), the precise mechanism of the multi-step reaction catalyzed by TIM is still under active discussion.

The other most-studied part of this enzyme is its catalytic loop 6 dynamics. McDermott and co-workers (12 and 13) have done elegant NMR studies on the motion of loop 6 and suggested that loop motion and product release are probably concerted and likely to represent a rate-limiting step for the catalytic reaction. However, the participation of loop 6 (residues 166–176) in positioning the catalytic base with suitable geometry, in protecting the reaction intermediates in its closed state, and in allowing ligand binding and release in its open state are not well understood. To enlighten on all these aspects of this enzyme, it is essential to have a pool of atomic resolution structures of the enzyme complexed with substrate and transition state analogues that will lead to an appreciation of the structural rearrangements at the active site during catalysis.

We present here the structural details at 1.1-Å resolution of *Plasmodium falciparum* (Pf) TIM complexed to an inhibitor 2-phosphoglycerate. Unlike the physiological substrate glyceraldehyde 3-phosphate, the phosphate group is attached to the C2 carbon in 2-phosphoglycerate (2PG) and has an additional negative charge and an extra oxygen atom (Fig. 1*b*). Earlier structural studies on PfTIM-ligand complexes (14, 15) suggest that a suitable substitution at the C2 carbon of 3PG could be potentially interesting as a lead for anti-malarial drug design. The structure of the PfTIM·2PG complex provides further insights on this possibility and shows how the interactions of the carboxy, phosphate, and hydroxyl groups of the ligand with the protein are altered due to change in the phosphate position. We also present a comparative analysis of this structure with the other two atomic resolution TIM structures, yeast TIM com-

* This work was supported by the Council of Scientific and Industrial Research, Government of India (to M. R. N. M.). The costs of publication of this article were defrayed in part by the payment of page charges. This article must therefore be hereby marked "*advertisement*" in accordance with 18 U.S.C. Section 1734 solely to indicate this fact.

The atomic coordinates and structure factors (code 1O5X) have been deposited in the Protein Data Bank, Research Collaboratory for Structural Bioinformatics, Rutgers University, New Brunswick, NJ (http://www.rcsb.org/).

§ Supported by the Council of Scientific and Industrial Research and in part by MAR Research.

‖ To whom correspondence should be addressed. Tel.: 91-80-2932458; Fax: 91-80-3600535 or 91-80-3600683; E-mail: mrn@mbu.iisc.ernet.in.

[1] The abbreviations used are: TIM, triose-phosphate isomerase; DHAP, dihydroxy acetone phosphate; PGA, phosphoglycolate; 2PG, 2-phosphoglycerate; LIGO and LIGC, 2-phosphoglycerate corresponding to the open and closed conformations of the catalytic loop, respectively; LBHB, low barrier hydrogen bond; Pf, *P. falciparum*.

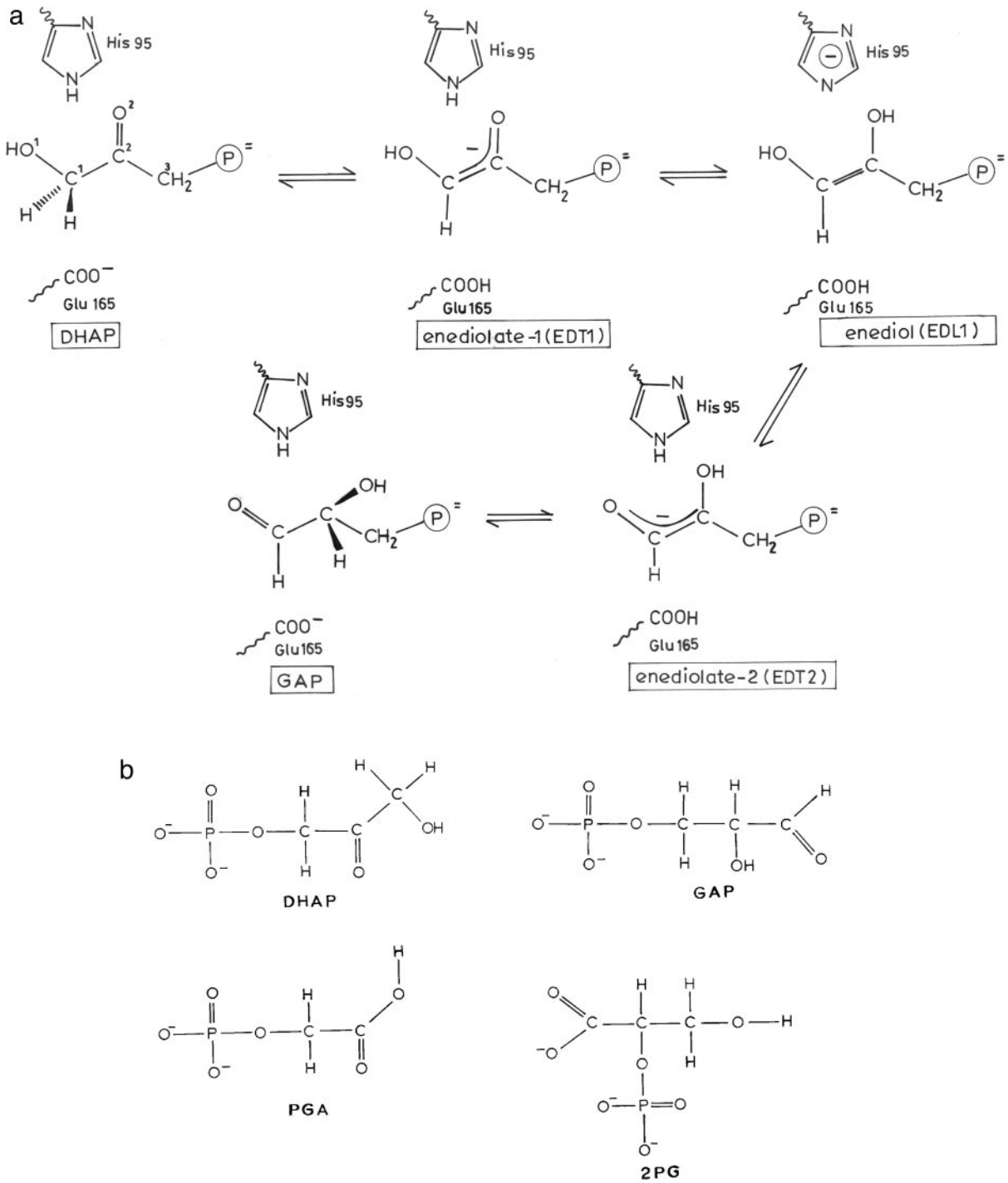

FIG. 1. *a*, structures of substrates and intermediates in TIM catalysis (3); *b*, structures of ligands in the known atomic resolution complexes of TIM. The terminal oxygen atoms of 2PG may be protonated at the pH of crystallization (pH 4.5). *GAP*, glyceraldehyde 3-phosphate.

plexed to the natural substrate DHAP (16) and *Leishmania mexicana* TIM complexed with the transition state analogue 2-phosphoglycolate (17).

EXPERIMENTAL PROCEDURES

Crystallization and Data Collection—Cloning, overexpression, and purification of PfTIM followed the procedures described earlier (18, 19). 2PG as the sodium salt was purchased from FLUKA chemicals. The purity of the sample was checked using electrospray ionization mass spectrometry and found to be nearly free of contaminants. Crystals of PfTIM·2PG complex were grown at the synchrotron station at EMBL-Hamburg using the hanging drop method. The reservoir solution contained 8–24% polyethylene glycol 1450 and 100 mM sodium acetate (pH 4–5.0). The protein concentration was 10 mg/ml. Protein and the ligand were mixed well, in molar ratios of either 1:50 or 1:100 before crystallization and allowed to equilibrate for 1 h. The cryoprotectant used was 20% glycerol dispersed in the crystallization buffer. Diffraction data were collected at 100 K at the X11 beam line of DESY maintained by EMBL-Hamburg. The wavelength of radiation was 0.9083 Å, produced using dosage mode. Reflections were recorded on a MAR165 mm CCD detector system. The data were processed using DENZO and scaled using SCALEPACK (20). The crystal belongs to the monoclinic $P2_1$ space group with a dimer in the asymmetric unit (see Table I).

Structure Solution and Refinement—The orientation and position of the dimeric molecule in the $P2_1$ cell were determined using the molecular replacement program AMoRe (21, 22) starting from the structure of native PfTIM determined at 2.1 Å (PDB code 1YDV) (19) as the phasing model. The molecular replacement model was improved by several rounds of refinement using CNS (23). Visual inspection of $2F_o - F_c$ and $F_o - F_c$ Fourier electron density maps and manual model

TABLE I
Data collection and refinement statistics of PfTIM-2PG complex

r.m.s.d., root mean square distance.

Intensity data statistics	
Radiation wavelength	1.1 Å
Space group	$P2_1$
Cell parameters	a = 54.49 Å b = 50.90 Å c = 89.01 Å β = 91.90°
Resolution range	30.0–1.1 Å
No. of reflections measured	777,359
No. of unique reflections	181,972
Overall completion	95.3%
Average $I/\sigma(I)$	13.88[a]
R_{symm}[b] (overall)	4.2%
R_{symm}[b] (1.12–1.10 Å)	46.4%
Completeness in 1.12–1.10 Å shell	87.3%
Refinement statistics	
R_{free} and R_{cryst} (final)	16.3 and 13.1 % (>4 σ) 17.1 and 13.3% (for all data)
r.m.s.d. in bond length	0.014 Å
r.m.s.d. in bond angle	2.256°
Anisotropy	
Protein	
Mean	0.427 Å^2
σ	0.0172 Å^2
Solvent	
Mean	0.389 Å^2
σ	0.142 Å^2
Ligand atoms	
Mean	0.374 Å^2
σ	0.183 Å^2
Mean isotropic equivalent B factor	
Protein	14.60 Å^2
Solvent	30.59 Å^2
Ligand atoms	28.57 Å^2

[a] Based on SHELXPRO analysis of .fcf file for 170,251 reflections.
[b] $R_{symm} = 100 \times \Sigma|I - I_h|/\Sigma I$.

rebuilding were performed with O and FRODO (24). The addition of ligands and 288 water molecules and refinement up to 1.1 Å resulted in R and R_{free} values of 0.235 and 0.247, respectively. Further refinement was continued with SHELX-97 (25), subjecting the structure to cycles of isotropic conjugate gradient least squares refinement. After extending the resolution to the limit of 1.1 Å and including several additional water molecules, R/R_{free} values were 0.178/0.199, respectively, for $F_o > 4\sigma(F_o)$. For further improvement of the model, tightly restrained anisotropic displacement parameters were introduced and refined as recommended (26, 27). This reduced both R and R_{free} values by ~3%. The final refinement cycle resulted in an R/R_{free} values of 0.133/0.171. The final refined structure was subjected to PROCHECK (28) for further assessment of errors. 433 of 450 non-glycine residues were found with (ϕ, ψ) values in the most favored region of the Ramachandran plot. 17 non-glycine residues were in the additional allowed region. The atomic resolution allowed detailed interpretation of electron density including chain disorder, anisotropy, and determination of specific ligand occupancies.

RESULTS

The final protein model obtained by refinement at 1.1 Å of resolution corresponds to R and R_{free} values of 13.3 and 17.1%, respectively, and has good stereochemical parameters (Table I). 96% of the protein residues lie in the most favored region of the Ramachandran map. The crystallographic asymmetric unit contains two subunits (A and B) related by a non-crystallographic 2-fold axis. In both the subunits the final refined electron density was unambiguous for most of the protein atoms except for a few side chains on the protein surface. Totally excluding the loop 6 residues, 11 residues in the A-subunit and 16 residues in the B-subunit were built in more than 1 conformation.

Despite the similar structures of the two subunits (root mean square distance for the superposition of all Cα positions (open form) is 0.25 Å), the electron densities at their active sites were considerably different. The electron density observed at the active site of the A-subunit did not account for an intact 2PG molecule but contained two pieces of unequal size. Careful examination of the interactions at the active site helps us to assign 2-oxoglycerate and *meta*-phosphate as plausible candidates for the larger and the smaller fragments, respectively. In this subunit, loop 6 is observed in an open conformation. In the B-subunit, the catalytic loop 6 has adopted both open and closed forms. The density fits the open conformation of loop 6 very well. The density corresponding to the closed conformation of loop 6 is well defined except for small breaks in the main chain density at residues 168, 170, and 172. There is no density for the side chain of Ile-170 in the closed form. The occupancies of the two conformations were restrained to add to unity in the refinement, which resulted in site occupancy of 0.62 for the open form. Consistent with the dual conformation of open and closed forms of loop 6 in the present case, residues 209–211 were also found in two conformations. In this subunit the electron density corresponding to the ligand at the active site was larger in extension than that of a single 2PG molecule. In addition, refinement of a fully occupied 2PG followed by difference Fourier calculation led to the appearance of negative electron density at the ligand surrounded by positive density, suggesting a partial occupancy for the built ligand. Systematic comparison of TIM complexes shows that the position of the phosphate moiety differs between the loop closed and the loop open forms of the enzyme (data not shown). The displacement of the phosphorous atom between the two forms is around 1.5 Å. Because loop 6 adopts both open and closed conformations in the B-subunit (see "Discussion") it may be anticipated that the ligand also has two orientations. Careful inspection of the features of the electron density map showed that this is indeed the case. These two orientations of 2PG are referred to as LIGO and LIGC, corresponding to loop open and closed forms respectively in the following paragraphs.

The mean anisotropy (26) of the protein atoms is 0.432 with

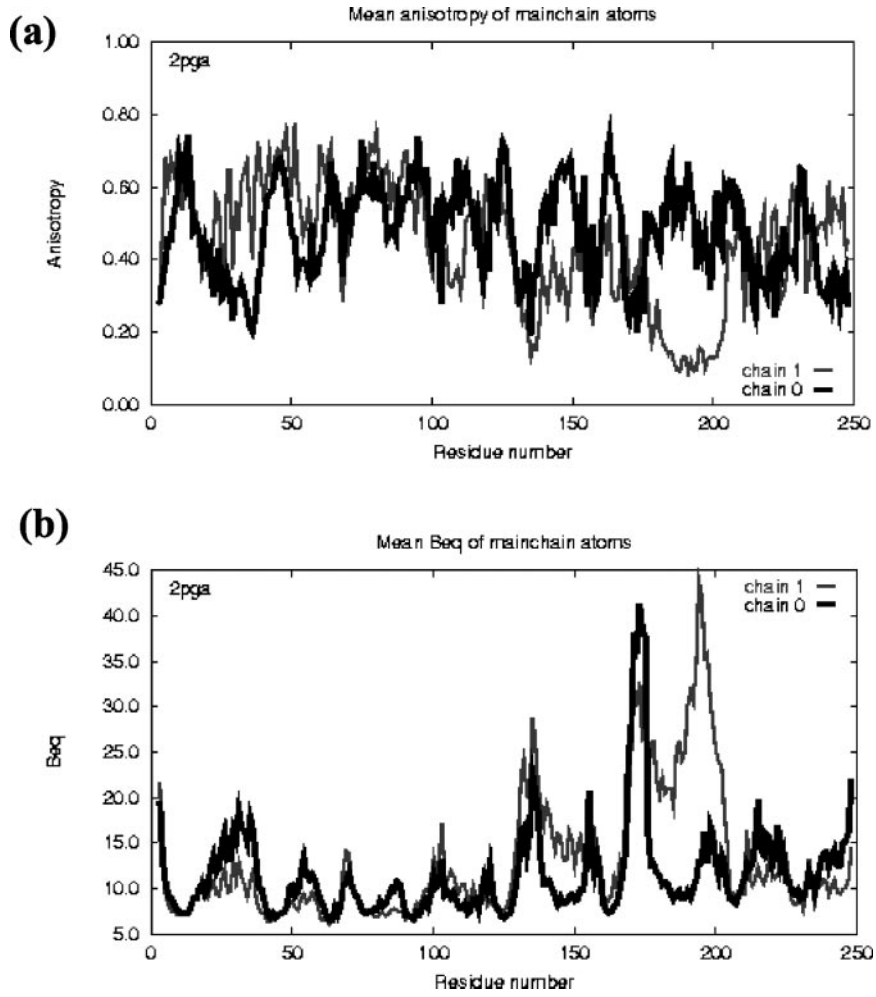

FIG. 2. *a*, distribution of mean anisotropy. *b*, mean B_{eq} as a function of the residue number. These plots were generated using PARVATI (26, 27).

a S.D. of 0.171. These correlate with the standard values (0.45, 0.15, respectively) as evaluated by Merritt (27). There is asymmetry of anisotropic displacement parameters of the main chain atoms between the subunits (Fig. 2*a*). The stretch of residues 180–200 shows the maximum difference in anisotropy between the subunits. These residues are more anisotropic in the B-subunit ($A < 0.2$) compared with the A-subunit ($A > 0.4$). The maximum anisotropy is observed for Lys-186 in the B-subunit (0.04). The isotropic thermal parameters also appear to be very high for these residues in the B-subunit compared with the A-subunit (Fig. 2*b*). Examination of the crystal packing for these residues suggests that the observed asymmetry could be an effect of the differences in crystal environment.

DISCUSSION

This high resolution structure determination of the complex 2-phosphoglycerate with *P. falciparum* triose-phosphate isomerase reveals the following features, 1) chemical cleavage of the ligand molecule bound to the A-subunit, presumably due to radiation damage, 2) predominance of the open conformation of catalytic loop 6 in the B-subunit, even in the presence of the bound ligand, a feature that appears to be a specific characteristic of the *Plasmodium* enzyme (14, 15) and the observation of two distinct conformations for several residues that correspond to open and closed forms of loop 6 at the active site of the B-subunit, and 3) the observation of two distinct positions for the ligand in the B-subunit. Each of these features is considered in detail.

Interpretation of the Fragmented Ligand Electron Density in Subunit A—The density at the active site of the A-subunit is fragmented and does not account for an intact 2PG molecule. The first impression obtained by the inspection of the fragmented density was that it might correspond to a glycerol used as the cryoprotectant and an acetate ion contained in the crystallization buffer. However, the density for glycerol was not symmetric about the C2 carbon; on the other hand, the branching at C1, which is expected for a carboxylate ion, was clearly visible (Fig. 3*a*). A second plausible interpretation of the density assigned the fragments as 2-oxoglycerate and *meta*-phosphate ion. The 2-oxoglycerate fits the larger fragment well. The identification of *meta*-phosphate ion as responsible for the smaller fragment is supported by the following. 1) One of the oxygen atoms, O1P, of the *meta*-phosphate interacts with OG atom of Ser-211. Another oxygen atom, O3P, shares a hydrogen bond with amide N of Asn-233. The position of this molecule is such that the third oxygen atom, O2P, points to the solvent region and could be hydrogen-bonded to a disordered solvent molecule. A weak hydrogen bond exists between this oxygen atom and ND2 of Asn-233. Also, various water-mediated hydrogen bonds made by O1P and O3P with the polypeptide stabilize the ion (Fig. 3*b*). 2) Although unstable, the occurrence of *meta*-phosphate has been proposed as an intermediate in reactions of phosphate monoesters based on various experiments (29).

The observed cleavage of 2PG into 2-oxoglycerate and *meta*-phosphate may be a consequence of damage due to the synchrotron radiation. Cleavage of the phosphorus-oxygen bond under such conditions has not been reported earlier. However, it is

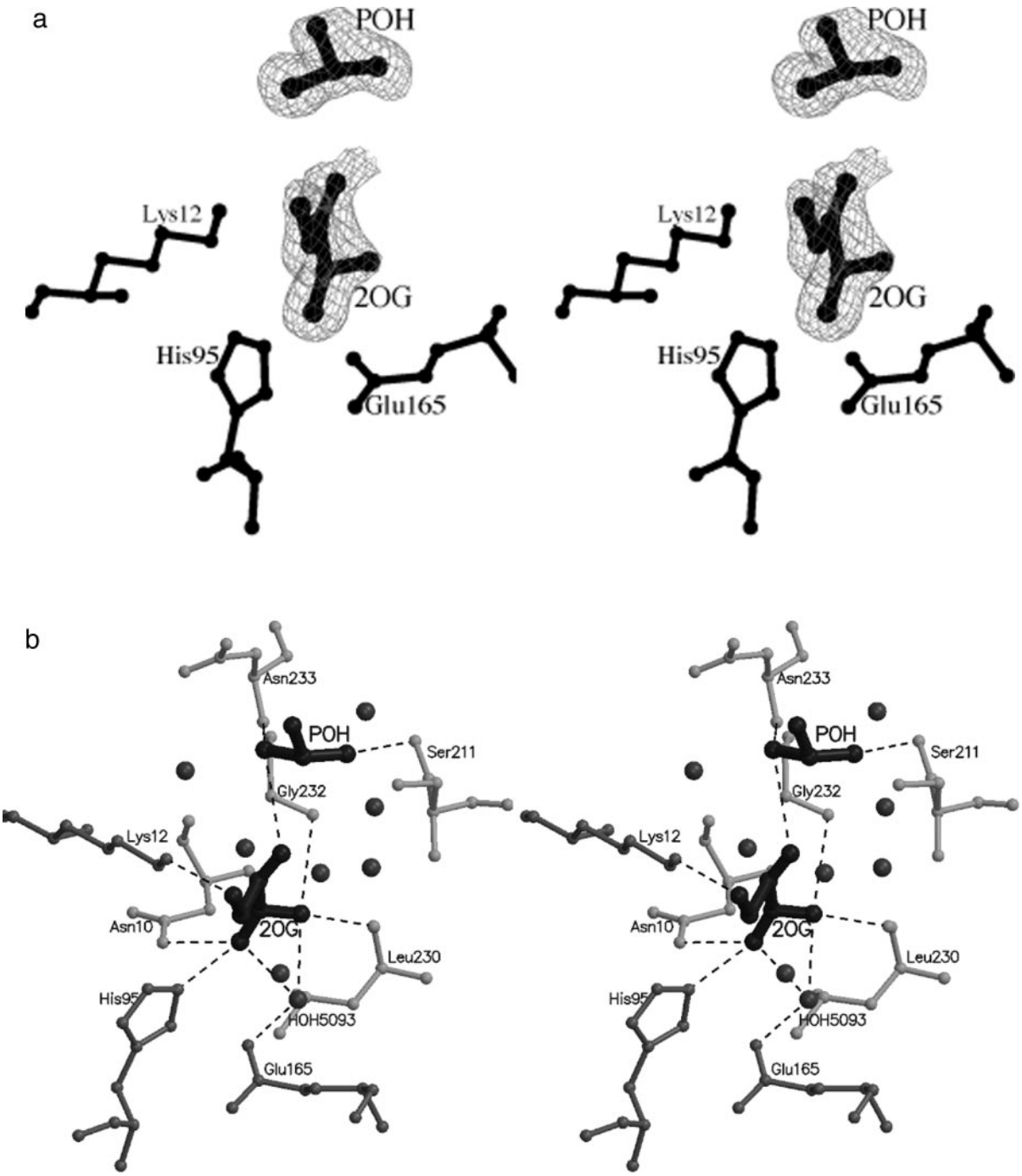

FIG. 3. *a*, stereo diagram illustrating the broken density corresponding to the ligand in the A-subunit of PfTIM·2PG complex. After completing the refinement of the complex, the fragments corresponding to the ligand were deleted, and the rest of the model was subjected to conjugate gradient least squares refinement in SHELX97. The figure shows the resulting $mF_o - DF_c$ σ-weighted map contoured at 2.5 σ. The catalytic residues are shown in *black*. The figure was generated using BOBSCRIPT. *b*, interactions of 2-oxoglycerate (*2OG*) and *meta*-phosphate ion (*POH*) in the A-subunit of PfTIM·2PG with the protein and water molecules. The hydrogen bonding interactions shown as *dotted lines* were identified by a distance criterion of 3.5 Å between suitable donor-acceptor atoms. The figure was generated using MOLSCRIPT.

known that exposure of bio-macromolecules to ionizing radiation results in damage (30–34). Some of the radiation induced damages commonly observed in protein structures even at cryogenic temperatures are cleavage of disulfide bonds (34), decarboxylation of acidic residues (35, 36), increase in atomic B-factors, and increase in unit cell volume (37). The present observation suggests that the energy-rich phosphoester bond is also susceptible to radiation damage.

It should be stressed that the *meta*-phosphate ion (monoanion, PO_3^-, or dianion, PO_3^{2-}) has been generally thought to be too unstable to exist in solution (38–40). An alternative fit to the smaller fragment of the electron density could be an acetate ion. In principle, the acetate ion would be anticipated to form two hydrogen-bonding interactions, in contrast to the *meta*-phosphate, which has three oxygen atoms available for accepting hydrogen bonds. Examination of the potential hydrogen-bonded interactions reveals that there are two strong bonds involving two of the phosphate oxygen atoms, whereas the third oxygen is close to the ND2 of Asn-233 (3.56 Å). This may or may not correspond to a hydrogen bond as the temperature factor of ND2 of Asn-233 is high (45 $Å^2$). However, the third oxygen atom is in contact with the solvent favoring its assign-

ment to a polar oxygen. In recent years, the structures of several chemically unstable reactive intermediates of carbenes and radicals have been characterized by x-ray analysis. It is therefore possible that the smaller density corresponds to an unstable *meta*-phosphate ion stabilized by favorable interactions with the proximal groups on the enzyme.

Conformations of the Catalytic Loop 6—It is believed that the catalytic loop 6 in TIM stabilizes the reaction intermediate and the transition states (41), protects the active site from contact with the bulk water (42), and prevents the phosphate elimination reaction (43). The dynamics of this loop in TIM have been probed by NMR and molecular dynamics studies (12, 13, 44–48). Solid state NMR experiments on yeast TIM (47) show that the loop motion is an inherent property of the protein and the time scale of the loop dynamics is of the order of 100 μs. Temperature-jump relaxation spectroscopy has recently been used to show that the substrate release is kinetically limited by loop opening (49). It was shown earlier that the stabilization of the closed form of the loop significantly contributes to TIM catalysis (50). This may not be true in the case of PfTIM as the structures of complexes of PfTIM with G3P and 3PG reported earlier (14, 15) suggest a preference of loop 6 for the open conformation. This prevalence of loop 6 in the open form in PfTIM can be attributed to the active site substitution found at the position 96. This residue is serine in all TIM sequences except *Plasmodium* species, where it is the more bulky phenylalanine. However, in the PGA complex of PfTIM, loop 6 is closed in the C2 form and open in the $P2_12_12_1$ form. Interestingly, in the present structure, loop 6 (B-subunit) has been observed in both conformations in the same crystal, although the loop open form is predominant.

The two conformations of loop 6 are correlated to features in other parts of the enzyme structure. The stretch of residues YGGS (208–211) is conserved in all the 73 distinct TIM sequences examined (data not shown). The closure and the concomitant changes bring about a number of new interactions between the flexible loop and these residues. In the B-subunit of PfTIM·2PG complex, where the loop 6 is in two conformations, residues 208–211 also exhibit dual conformations, of which one corresponds to the loop open and the other to the loop closed forms. One of the conformations of Ser-211 makes strong hydrogen bonds with the residues at the tip of loop 6. The other residues, Tyr-208, Gly-209, and Gly-210, also contribute significantly to the stabilization of the loop in the closed conformation. It has been shown from molecular dynamics simulations (48) that the hydrogen bond between Tyr-208 and the loop residue Ala-176 plays a crucial role in the loop opening and closing mechanism. In the A-subunit there is only one conformation for this stretch, and that corresponds to the loop open form. The position of Phe-96 as observed in the loop open conformation makes severe short contacts with the closed loop. This steric clash with Ile-170 of loop 6 results in an altered conformation of Phe-96 upon loop closure (15). However, this altered position overlaps with the position of the side chain of Leu-167 in the open form of the loop. Hence, loop closure also leads to repositioning of the Leu-167 side chain. In the B-subunit the densities corresponding to the alternate conformations of Phe-96 and Leu-167 are also present. As anticipated, the density corresponding to the preponderant open loop form is better-defined. In contrast these two residues are in a single conformation in the A-subunit where loop 6 is only in the open form. Another distinct difference between the open and closed loop conformations is the position of the ligand, and in particular, the position of the phosphate group. In the B-subunit, the density at the active site evidently fits these two orientations of the ligand, as discussed below.

The chemical features that restrain the loop opening are not entirely clear. The most likely constraint for loop motion is the environment of loop 6, consisting of the ligand and the nearby acidic and basic groups (49). Spectroscopic studies on TIM from *Saccharomyces cerevisiae* suggest opening and closing rates of 2500 ± 1000 and $46{,}700 \pm 1800$ s^{-1}, respectively. The higher rate for the closure of loop 6 probably ensures the protection of the active site while making and releasing the products (49). A further observation from solid state NMR experiments on yeast TIM is that the opening rate depends on the chemical nature of the binding ligand; slower opening rates are associated with stronger binding ligands (12). The observation of loop 6 predominantly in open conformation in this complex and various other complexes of PfTIM suggest that the catalytic loop dynamics in PfTIM is likely to be distinctly different from other TIMs and that the rate of loop opening might be higher than that of closure.

Multiple Bound Ligand Conformations in Subunit B—Fig. 4*a* shows two distinct orientations of 2PG modeled into the ligand electron density at the active site of the B-subunit. The most significant feature of the ligand that could be inferred from the electron density is the near planarity of bonds at the C2 position in LIGC, which is in sharp contrast to the tetrahedral geometry observed in the trypanosomal TIM·2PG complex (51), as expected for an sp^3-hybridized carbon atom.

Numerous interactions stabilize LIGO and LIGC in the B-subunit. Figs. 4, *b* and *c*, show the stereo view of the interactions between atoms of LIGO and LIGC, respectively, and the polypeptide. The phosphate group is involved in numerous direct and water-mediated interactions with two stretches of residues, Gly-209–Val-212 and the residues of the phosphate binding helix, Leu-230–Ala-234. In its major conformation, the OG atom of Ser-211 interacts directly with the phosphate group of LIGO. In the minor conformation this atom is hydrogen-bonded to the phosphate group of LIGC through a water molecule. The features such as direct hydrogen bonding between the phosphate oxygen atoms of the ligand and the main chain O and N atoms of Gly-232, Asn-233, and Ser-211 as observed in other PfTIM-ligand complexes are found with both orientations of the ligand.

Unlike subunit-A, the presence of an intact ligand in subunit-B suggests that there is asymmetry in the extent of binding of the ligands to the active sites of the dimeric enzyme, a feature observed in other PfTIM complexes also (14, 15). This asymmetry has been observed earlier in trypanosomal TIM complexed with various ligands but appears to be a result of crystallographic contacts (52, 53). In PfTIM, asymmetry seems to be an intrinsic, although puzzling property not related to crystallographic packing. To analyze the plausible source of this asymmetry, all the residues within a radius of 6 Å from the ligand were examined. This distance limit included all residues that could interact directly or through water-mediated interactions with the ligand. It was found that two such residues, Asn-233 of the same subunit and Ser-73 of the symmetry-related subunit, are Gly and Ala in most of the TIM sequences from other sources. Except for these two, all the other residues are conserved (data not shown). Ser-73 is located in loop 3, which protrudes from one subunit and approaches the active site of the other subunit. The water-mediated hydrogen-bonding interaction of Ser-73 with the ligand (from the symmetry related subunit) maintains the dimeric symmetry of PfTIM. On the contrary, Asn-233 of the A-subunit is hydrogen-bonded through a water molecule to Ser-73 of the B-subunit, whereas Asn-233 of the B-subunit makes a direct hydrogen bond with Ser-73 of the A-subunit (Fig. 5). This is presumably due to differences in the hydration at the active sites of the two

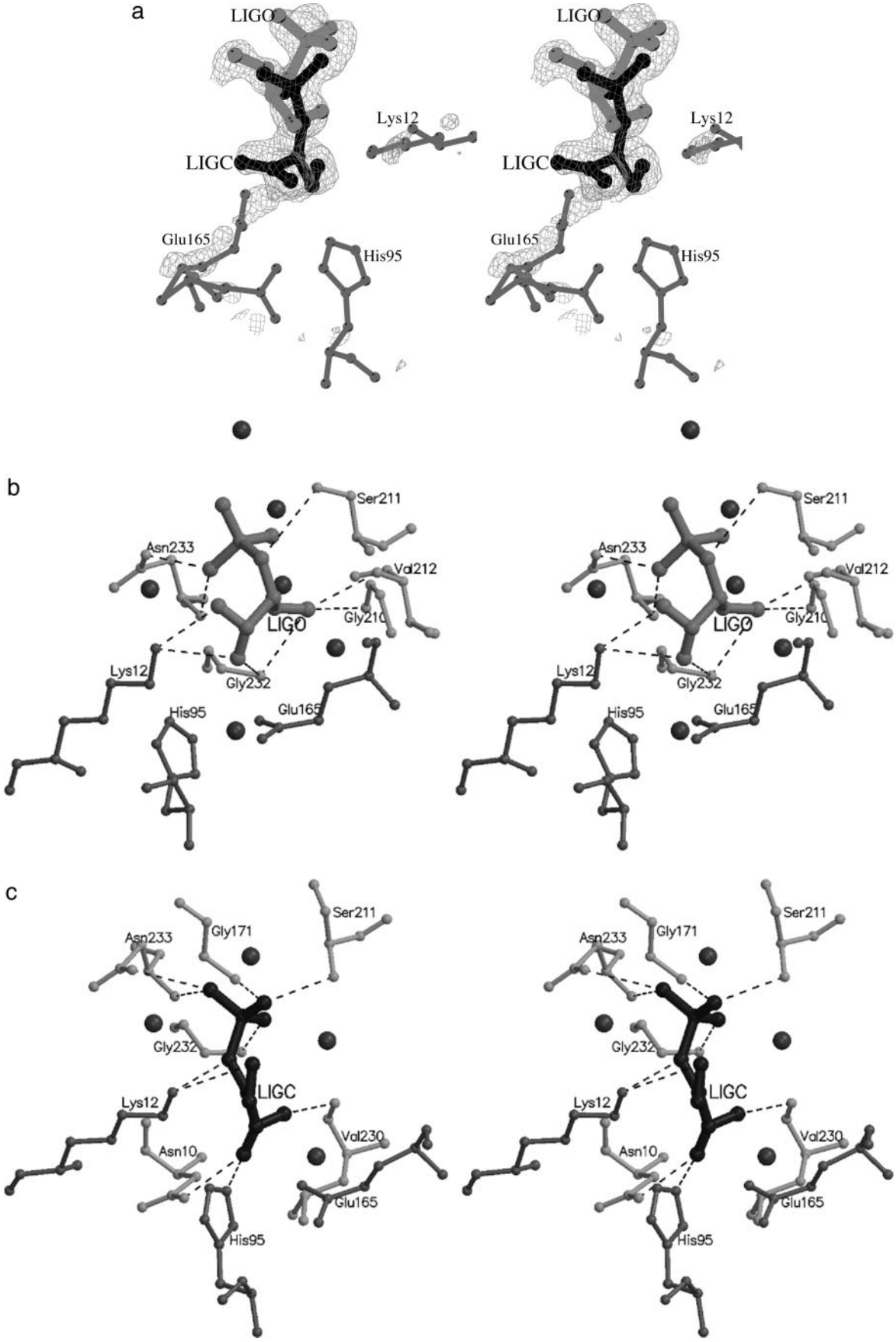

FIG. 4. *a*, stereo view of the active site of the B-subunit of PfTIM·2PG complex. The figure shows the fit of the ligand to the difference Fourier electron density map ($mF_o - DF_c$; 2.5 σ) calculated with the phases obtained after refinement without the ligand. LIGO and LIGC correspond to loop open and closed forms, respectively. LIGO is shown in *gray*, and LIGC is shown in *black*. *b*, interactions of LIGO bound to the B-subunit of PfTIM·2PG complex. *c*, interactions of LIGC in the same subunit. The hydrogen bonds shown as *dotted lines* are the contacts between the appropriate donor-acceptor pairs within a distance limit of 3.5 Å. The catalytic residues are shown in *black*.

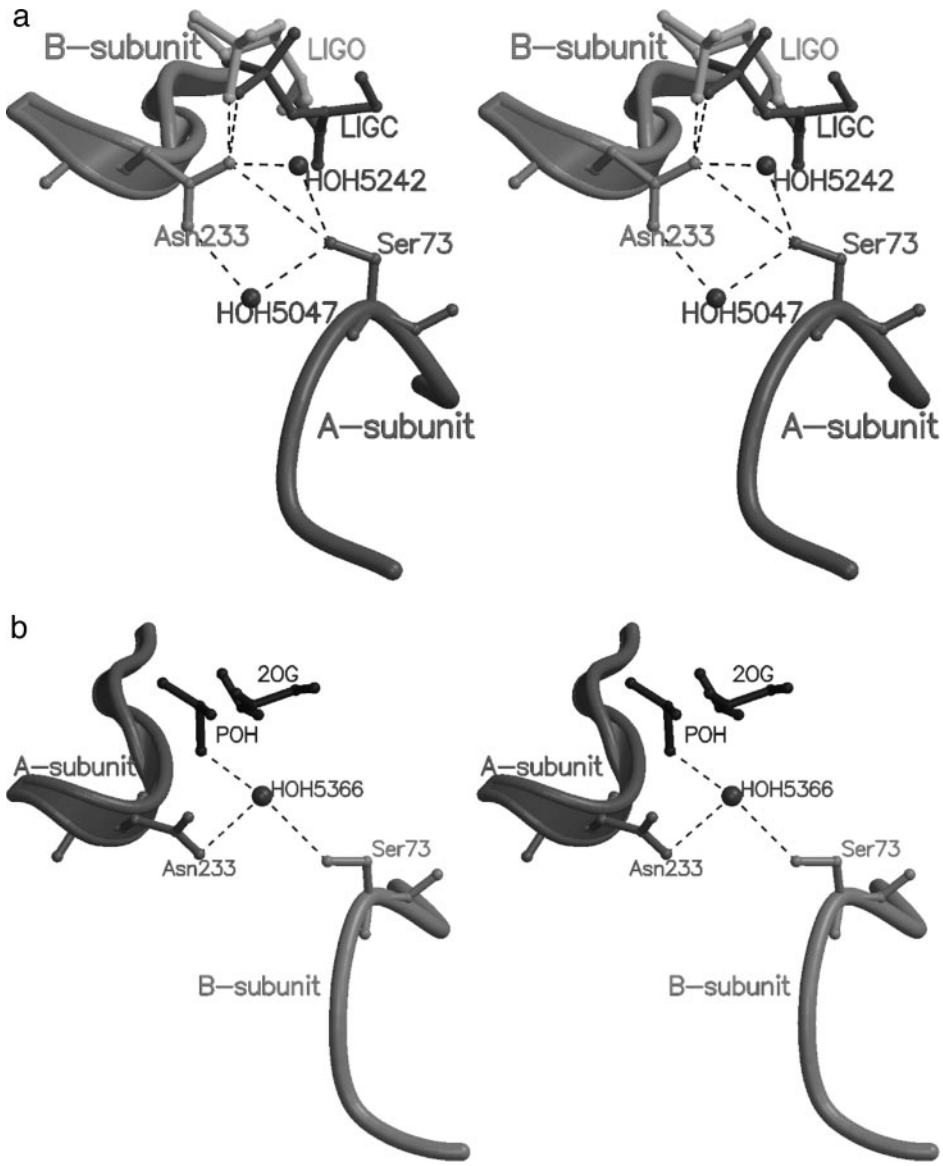

FIG. 5. **Interactions of Asn-233 with Ser-73 from the symmetry-related subunit in the PfTIM·2PG complex.** *a*, the active site of the B-subunit. OD1 of Asn-233 forms a direct hydrogen bond with OG of Ser-73 of the A-subunit. *b*, in the A-subunit Asn-233 interacts with Ser-73 of the B-subunit only through a water molecule. These differences between the subunits are probably due to the rearrangement of water molecules upon ligand binding. The figure was prepared using MOLSCRIPT. *POH*, *meta*-phosphate ion; *2OG*, 2-oxoglycerate.

subunits, which may result from the sequence of ligand binding to the subunits. These observations need further confirmation by investigations on ligand complexes of site-specific mutants of these residues.

Interactions between Phe-96 and the ligands in other PfTIM complexes suggest that the substitution of non-polar groups at C2 might serve as potent inhibitors of the enzyme. In the present structure, C2 is bonded to a highly polar phosphate group. This results in a twist of the ligand such that now the C3 carbon points toward Phe-96. This observation further suggests the importance of Phe-96 in PfTIM for the design of anti-malarial compounds.

Comparison of the Active Site with Other High Resolution Structures and Implication for Catalysis—Apart from the present structure, two others, yeast TIM·DHAP complex and *L. mexicana* E65Q mutant complexed with the transition state analogue, 2-phosphoglycolate, are available at ultrahigh resolution. Detailed comparison of all these structures brings to light many interesting aspects of TIM catalysis. By careful temperature-controlled retardation of catalysis, the ligand was trapped as the Michaelis complex at the active site of yeast TIM·DHAP determined at 1.2-Å resolution (16) (hereafter, DHAP complex). In the 0.83-Å resolution structure of the *L. mexicana* E65Q mutant-2 phosphoglycolate complex, two conformations of the triose moiety with features resembling those suggested for the transition state were observed (17) (hereafter, PGA complex). These structures suggest that the transition state of the catalytic reaction in TIM represents a metastable intermediate. Although the ligand 2-phosphoglycerate is an inhibitor, the protein-ligand interactions in the present case (hereafter, 2PG complex) partly resemble those of the other two complexes.

The catalytic residue Glu-165 was observed in two conformations with a separation of ~2 Å between the terminal carboxylates. These conformations are usually associated with the open and closed forms of loop 6. The transition in the position of Glu-165 upon ligand binding and loop closure facilitates proton transfer between C1 and C2 centers of the ligand. The major conformation of Glu-165 does not interact with the ligand; the carboxylate of Glu-165 is at a distance more than 4.5 Å from the ligand. In its minor conformation, OE2 of Glu-165 makes short and strong interactions with LIGC. These strong

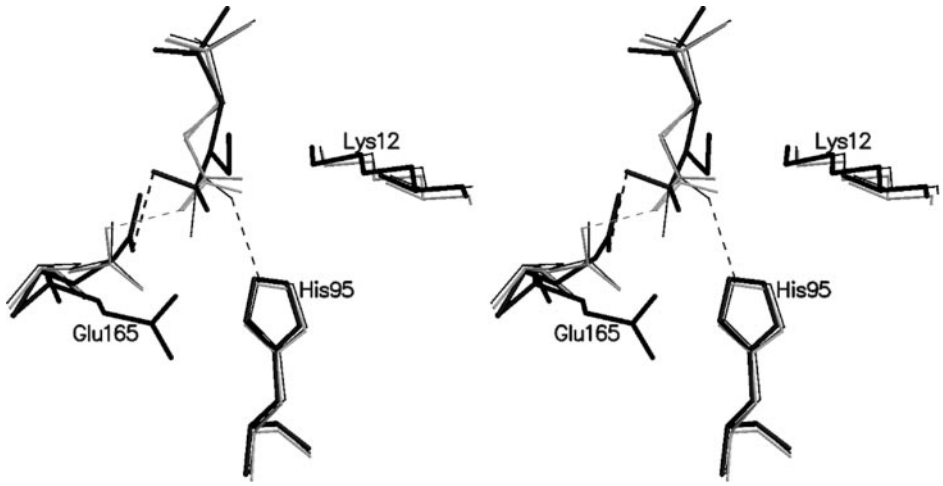

FIG. 6. **Stereo view illustrating the key interactions at the active sites of 2PG, PGA, and DHAP complexes (see "Discussion" for definition).** The structure of 2PG complex was used as the reference model onto which the other two structures were superposed. The segments of DHAP, PGA, and 2PG complexes are represented by *thin black*, *thin gray*, and *thick back sticks*. The low barrier hydrogen bonds are represented by *dotted lines*. Water molecules located in the active site of the 2PG complex are not shown for clarity.

hydrogen bonds, which Cleland (2) has termed "low barrier hydrogen bonds" (LBHB), have energies of formation in the range of 10–20 kcal mol^{-1}. This energy is thought to facilitate the catalysis by lowering the free energy of the transition state. Such a LBHB is observed in the DHAP complex between the imidazole of His-95 with the ketone oxygen of the substrate (2.56 Å; Fig. 6). In the PGA complex, however, the corresponding distances are 2.74 and 3.39 Å for the two conformations of the ligand, respectively. In the 2PG complex the conformation of His-95 is similar to that of the other two complexes. NE2 of His-95 is at 2.98 Å from O11 of LIGC, which is of the order found in the PGA complex, and these hydrogen bonds do not represent LBHBs. Nevertheless, in the PGA complex, a LBHB is observed between OE2 of Glu-165 and O1 atom of PGA in both of its conformations (2.61 and 2.59 Å). In the DHAP complex, there is no LBHB between Glu-165 and the substrate; the carboxylate oxygen atom is at 3.0 Å from the hydroxyl oxygen of the substrate. Interestingly, in the present structure, OE2 of Glu-165 forms a LBHB with O12 of LIGC (2.64 Å) similar to the PGA complex. Also, OE1 and OE2 of Glu-165 are very close (<3 Å) from all the three carbon atoms of 2PG, representing unusual CH···O hydrogen bonds. Similar hydrogen bonds have also been observed in the DHAP complex between the OE2 oxygen of Glu-165 and the C1 and C2 atoms of DHAP (3.0 Å). It is believed that Glu-165 and His-95 are the most likely residues facilitating the first and the second proton transfers, respectively, in TIM catalysis (3, 54). The activation barrier for these proton transfers could be considerably lowered by these short, strong hydrogen bonds (3). The atomic resolution structure presented here along with the other two high resolution structures provides evidence for the anticipated LBHBs at the active site of TIM.

The ultra-high resolution structural information presented here provides insights into the features of the malarial enzyme. The presence of *meta*-phosphate anion at the active site of one of the subunits generated by the radiation cleavage of the bound 2-phosphoglycerate was observed for the first time in protein structures. The observation of dual conformations of the bound ligand correlates with the observed dual conformation of loop 6. Although 2PG is neither a substrate nor a transition state analogue, the identification of an LBHB between the ligand and the catalytic base Glu-165 and other interactions at the active site resemble those in the high resolution structures of other TIM complexes and support the proposed importance of substrate placed at suboptimal position and strong interactions with the intermediate as essential features of TIM catalysis.

Acknowledgments—Preliminary examination of PfTIM·2PG complex was carried out at the x-ray facility for Structural Biology at the Molecular Biophysics Unit of the Indian Institute of Science supported by the Department of Science and Technology and the Department of Biotechnology. Use of the facilities at the Supercomputer Education and Research Centre, Interactive Graphics Based Molecular Modeling Facility, and the Bioinformatics Centre (supported by the Department of Science and Technology) are acknowledged. We acknowledge the assistance of James Paul and P. F. Babu during the course of these investigations. We are thankful to Dr. Victor Lamzin and Dr. Paul Tucker for helping with data collection on the X11 beam line of DESY, Hamburg.

REFERENCES

1. Knowles, J. R. (1991) *Nature* **350,** 121–124
2. Cleland, W. W. & Kreevoy, M. M. (1994) *Science* **264,** 1887–1890
3. Cui, Q. & Karplus, M. (2001) *J. Am. Chem. Soc.* **123,** 2284–2290
4. Herlihy, J. M., Maister, S. G., Albery, W. J. & Knowles, J. R. (1976) *Biochemistry* **15,** 5601–5607
5. Albery, W. J. & Knowles, J. R. (1976) *Biochemistry* **15,** 5627–5631
6. Lolis, E. & Petsko, G. A. (1990) *Biochemistry* **29,** 6619–6625
7. Komives, E. A., Chang, L. C., Lolis, E., Tilton, R. F., Petsko, G. A. & Knowles, J. R. (1991) *Biochemistry* **30,** 3011–3019
8. Harris, T. K., Cole, R. N., Comer, F. I. & Mildvan, A. S. (1998) *Biochemistry* **37,** 16828–16838
9. Davenport, R. C., Bash, P. A., Seaton, B. A., Karplus, M., Petsko, G. A. & Ringe, D. (1991) *Biochemistry* **30,** 5821–5826
10. Bash, P. A., Field, M. J., Davenport, R. C., Petsko, G. A., Ringe, D. & Karplus, M. (1991) *Biochemistry* **30,** 5826–5832
11. Aqvist, J. & Fothergill, M. (1996) *J. Biol. Chem.* **271,** 10010–10016
12. Rozovsky, S., Jogl, G., Tong, L. & McDermott, A. E. (2001) *J. Mol. Biol.* **310,** 271–280
13. Rozovsky, S. & McDermott, A. E. (2001) *J. Mol. Biol.* **310,** 259–270
14. Parthasarathy, S., Balaram, H., Balaram, P. & Murthy, M. R. (2002) *Acta Crystallogr. Sect. D Biol. Crystallogr.* **58,** 1992–2000
15. Parthasarathy, S., Ravindra, G., Balaram, H., Balaram, P. & Murthy, M. R. (2002) *Biochemistry* **41,** 13178–13188
16. Jogl, G., Rozovsky, S., McDermott, A. E. & Tong, L. (2003) *Proc. Natl. Acad. Sci. U. S. A.* **100,** 50–55
17. Kursula, I. & Wierenga, R. K. (2003) *J. Biol. Chem.* **278,** 9544–9551
18. Ranie, J., Kumar, V. P. & Balaram, H. (1993) *Mol. Biochem. Parasitol.* **61,** 159–169
19. Velanker, S. S., Ray, S. S., Gokhale, R. S., Suma, S., Balaram, H., Balaram, P. & Murthy, M. R. (1997) *Structure* (*Lond.*) **5,** 751–761
20. Otwinowsky, Z. & Minor, W. (1997) *Methods Enzymol.* **276,** 307–326
21. Navaza, J. (1994) *Acta Crystallogr. Sect. A* **50,** 157–163
22. Navaza, J. & Saludjian, P. (1997) *Methods Enzymol.* **276,** 581–593
23. Brunger, A. T., Adams, P. D., Clore, G. M., DeLano, W. L., Gros, P., Grosse-Kunstleve, R. W., Jiang, J. S., Kuszewski, J., Nilges, M., Pannu, N. S., Read, R. J., Rice, L. M., Simonson, T. & Warren, G. L. (1998) *Acta Crystallogr. Sect. D* **54,** 905–921
24. Jones, T. A., Zou, J. Y., Cowan, S. W. & Kjeldgaard. (1991). *Acta Crystallogr. Sect. A* **47,** 110–119
25. Sheldrick, G. M. & Schneider, T. R. (1997) *Methods Enzymol.* **277,** 319–343
26. Merritt, E. A. (1999) *Acta Crystallogr. Sect. D* **55,** 1997–2004
27. Merritt, E. A. (1999) *Acta Crystallogr. Sect. D* **55,** 1109–1117
28. Laskowski, R. A., Moss, D. S. & Thornton, J. M. (1993) *J. Mol. Biol.* **231,**

1049–1067
29. Butcher, W. W. & Westheimer, F. H. (1955) *J .Am. Chem. Soc.* **77,** 2420–2424
30. Kumamoto, J. & Westheimer, F. H. (1955) *J. Am. Chem. Soc.* **77,** 2515–2518
31. Hedman, B., Hodgson, K. O., Helliwell, J. R., Liddington, R. & Papiz, M. Z. (1985) *Proc. Natl. Acad. Sci. U. S. A.* **82,** 7604–7607
32. Weik, M., Ravelli, R. B., Kryger, G., McSweeney, S., Raves, M. L., Harel, M., Gros, P., Silman, I., Kroon, J. & Sussman, J. L. (2000) *Proc. Natl. Acad. Sci. U. S. A.* **97,** 623–628
33. Matsui, Y., Sakai, K., Murakami, M., Shiro, Y., Adachi, S., Okumura, H. & Kouyama, T. (2002) *J. Mol. Biol.* **324,** 469–481
34. Schroder Leiros, H. K., McSweeney, S. M. & Smalas, A. O. (2001) *Acta Crystallogr. Sect. D* **57,** 488–497
35. Burmeister, W. P. (2000) *Acta Crystallogr. Sect. D* **56,** 328–341
36. Ravelli, R. B. & McSweeney, S. M. (2000) *Structure Fold. Des.* **8,** 315–328
37. Ravelli, R. B., Theveneau, P., McSweeney, S. & Caffrey, M. (2002) *J. Synchrotron Radiat.* **9,** 355–360
38. Bourne, N. & Williams, A. (1984) *J. Am. Chem. Soc.* **106,** 7591–7596
39. Skoog, M. T. & Jencks, W. P. (1984) *J. Am. Chem. Soc.* **106,** 7597–7606
40. Herschlag, D. & Jencks, W. P. (1990) *Biochemistry* **29,** 5172–5179
41. Joseph-McCarthy, D., Lolis, E., Komives, E. A. & Petsko, G. A. (1994) *Biochemistry* **33,** 2815–2823
42. Pompliano, D. L., Peyman, A. & Knowles, J. R. (1990) *Biochemistry* **29,** 3186–3194
43. Lolis, E., Alber, T., Davenport, R. C., Rose, D., Hartman, F. C. & Petsko, G. A. (1990) *Biochemistry* **29,** 6609–6618
44. Joseph, D., Petsko, G. A. & Karplus, M. (1990) *Science* **249,** 1425–1428
45. Wade, R. C., Davis, M. E., Luty, B. A., Madura, J. D. & McCammon, J. A. (1993) *Biophys. J.* **64,** 9–15
46. Wade, R. C., Luty, B. A., Demchuk, E., Madura, J. D., Davis, M. E., Briggs, J. M. & McCammon, J. A. (1994) *Nat. Struct. Biol.* **1,** 65–69
47. Williams, J. C. & McDermott, A. E. (1995) *Biochemistry* **34,** 8309–8319
48. Derreumaux, P. & Schlick, T. (1998) *Biophys. J.* **74,** 72–81
49. Desamero, R., Rozovsky, S., Zhadin, N., McDermott, A. & Callender, R. (2003) *Biochemistry* **42,** 2941–2951
50. Sampson, N. S. & Knowles, J. R. (1992) *Biochemistry* **31,** 8482–8487
51. Noble, M. E., Verlinde, C. L., Groendijk, H., Kalk, K. H., Wierenga, R. K. & Hol, W. G. (1991) *J. Med. Chem.* **34,** 2709–2718
52. Wierenga, R. K., Noble, M. E., Vriend, G., Nauche, S. & Hol, W. G. (1991) *J. Mol. Biol.* **220,** 995–1015
53. Noble, M. E., Wierenga, R. K., Lambeir, A. M., Opperdoes, F. R., Thunnissen, A. M., Kalk, K. H., Groendijk, H. & Hol, W. G. (1991) *Proteins* **10,** 50–69
54. Albery, W. J. & Knowles, J. R. (1976) *Biochemistry* **15,** 5588–6000